



UNIVERSITY OF LEEDS

This is a repository copy of *CH<sub>2</sub>OO Criegee intermediate UV absorption cross-sections and kinetics of CH<sub>2</sub>OO + CH<sub>2</sub>OO and CH<sub>2</sub>OO + I as a function of pressure.*

White Rose Research Online URL for this paper:  
<http://eprints.whiterose.ac.uk/159396/>

Version: Supplemental Material

---

**Article:**

Mir, ZS [orcid.org/0000-0003-2223-2833](https://orcid.org/0000-0003-2223-2833), Lewis, TR, Onel, L et al. (3 more authors) (2020) CH<sub>2</sub>OO Criegee intermediate UV absorption cross-sections and kinetics of CH<sub>2</sub>OO + CH<sub>2</sub>OO and CH<sub>2</sub>OO + I as a function of pressure. *Physical Chemistry Chemical Physics*, 22 (17). pp. 9448-9459. ISSN 1463-9076

<https://doi.org/10.1039/D0CP00988A>

---

This journal is © the Owner Societies 2020. This is an author produced version of an article published in *Physical Chemistry Chemical Physics*. Uploaded in accordance with the publisher's self-archiving policy.

**Reuse**

Items deposited in White Rose Research Online are protected by copyright, with all rights reserved unless indicated otherwise. They may be downloaded and/or printed for private study, or other acts as permitted by national copyright laws. The publisher or other rights holders may allow further reproduction and re-use of the full text version. This is indicated by the licence information on the White Rose Research Online record for the item.

**Takedown**

If you consider content in White Rose Research Online to be in breach of UK law, please notify us by emailing [eprints@whiterose.ac.uk](mailto:eprints@whiterose.ac.uk) including the URL of the record and the reason for the withdrawal request.



[eprints@whiterose.ac.uk](mailto:eprints@whiterose.ac.uk)  
<https://eprints.whiterose.ac.uk/>

# CH<sub>2</sub>OO Criegee Intermediate UV absorption cross-sections and kinetics of CH<sub>2</sub>OO + CH<sub>2</sub>OO and CH<sub>2</sub>OO + I as a function of pressure

Zara S. Mir,<sup>1</sup> Thomas R. Lewis,<sup>1</sup> Lavinia Onel,<sup>1</sup> Mark A. Blitz,<sup>1,2</sup> Paul W. Seakins,<sup>1</sup> Daniel Stone<sup>1\*</sup>

<sup>1</sup>School of Chemistry, University of Leeds, <sup>2</sup>National Centre for Science, University of Leeds

\*Corresponding author: [d.stone@leeds.ac.uk](mailto:d.stone@leeds.ac.uk)

## Supplementary Information

### Determination of $\sigma_{\text{CH}_2\text{OO,max}} [\text{CH}_2\text{OO}]_{t=0} l$ and $\sigma_{\text{CH}_2\text{OO,max}}$

The product  $\sigma_{\text{CH}_2\text{OO,max}} [\text{CH}_2\text{OO}]_t l$  was determined as described in the main text, where  $\sigma_{\text{CH}_2\text{OO,max}}$  is the peak CH<sub>2</sub>OO UV absorption cross-section,  $[\text{CH}_2\text{OO}]_t$  is the concentration of CH<sub>2</sub>OO, and  $l$  is the effective path length of the probe beam through the reaction cell.

The initial concentration of CH<sub>2</sub>OO was determined from the observed depletion of CH<sub>2</sub>I<sub>2</sub>, which gives the initial concentration of CH<sub>2</sub>I radicals, and our previous measurements of CH<sub>2</sub>OO yields from CH<sub>2</sub>I + O<sub>2</sub> as a function of pressure.<sup>1</sup> In order to determine  $\sigma_{\text{CH}_2\text{OO,max}} [\text{CH}_2\text{OO}]_{t=0} l$ , and thus  $\sigma_{\text{CH}_2\text{OO,max}}$ , it was necessary to fit the time profile for the absorbance at the wavelength at which the maximum cross-section is observed,  $A_{t,\lambda,\text{max}} = \sigma_{\text{CH}_2\text{OO,max}} [\text{CH}_2\text{OO}]_t l$ , to a mixed first- and second-order kinetic loss equation (Equation S1):

$$A_{t,\lambda,\text{max}} = \frac{k_1 A_{0,\lambda,\text{max}}}{k_1 e^{k_1 t} - 2 \left( \frac{k_2}{\sigma_{\text{CH}_2\text{OO,max}} l} \right) A_{0,\lambda,\text{max}} + 2 \left( \frac{k_2}{\sigma_{\text{CH}_2\text{OO,max}} l} \right) A_{0,\lambda,\text{max}} e^{k_1 t}} \quad (\text{Equation S1})$$

where  $A_{0,\lambda,\text{max}} = \sigma_{\text{CH}_2\text{OO,max}} [\text{CH}_2\text{OO}]_0 l$  (the value of  $[\text{CH}_2\text{OO}]_0 l$  is determined from the observed product of the depletion of CH<sub>2</sub>I<sub>2</sub> and path length,  $\Delta[\text{CH}_2\text{I}_2] l$ , and the pressure dependent CH<sub>2</sub>OO yield from CH<sub>2</sub>I + O<sub>2</sub>),  $k_1$  is the first-order loss component for CH<sub>2</sub>OO, primarily resulting from diffusion out of the probe beam, and  $k_2$  is the second order loss component for CH<sub>2</sub>OO owing to both the CH<sub>2</sub>OO self-reaction and the reaction of CH<sub>2</sub>OO + I. Figure S1 shows the fit result.

The effective path length,  $l$ , was determined from experiments in which the absorbance owing to IO from a single pass of the probe beam through the reaction cell, which overlapped completely with the photolysis laser and thus has a path length equal to the 1.5 m length of the reaction cell, was compared to the absorbance owing to IO measured simultaneously from the multipass arrangement. For seven passes of the probe beam through the cell,  $l$  was determined to be  $(443 \pm 21)$  cm, and for thirteen passes of the probe beam through the cell,  $l$  was determined to be  $(1136 \pm 143)$  cm. Although the path length,  $l$ , was experimentally determined for these configurations of the probe beam, it should be noted that the determination of  $\sigma_{\text{CH}_2\text{OO,max}}$  is independent of the path length in this analysis.

1. Stone, D.; Blitz, M.; Daubney, L.; Ingham, T.; Seakins, P. CH<sub>2</sub>OO Criegee biradical yields following photolysis of CH<sub>2</sub>I<sub>2</sub> in O<sub>2</sub>. *Physical Chemistry Chemical Physics* **2013**, *15* (44), 19119-19124

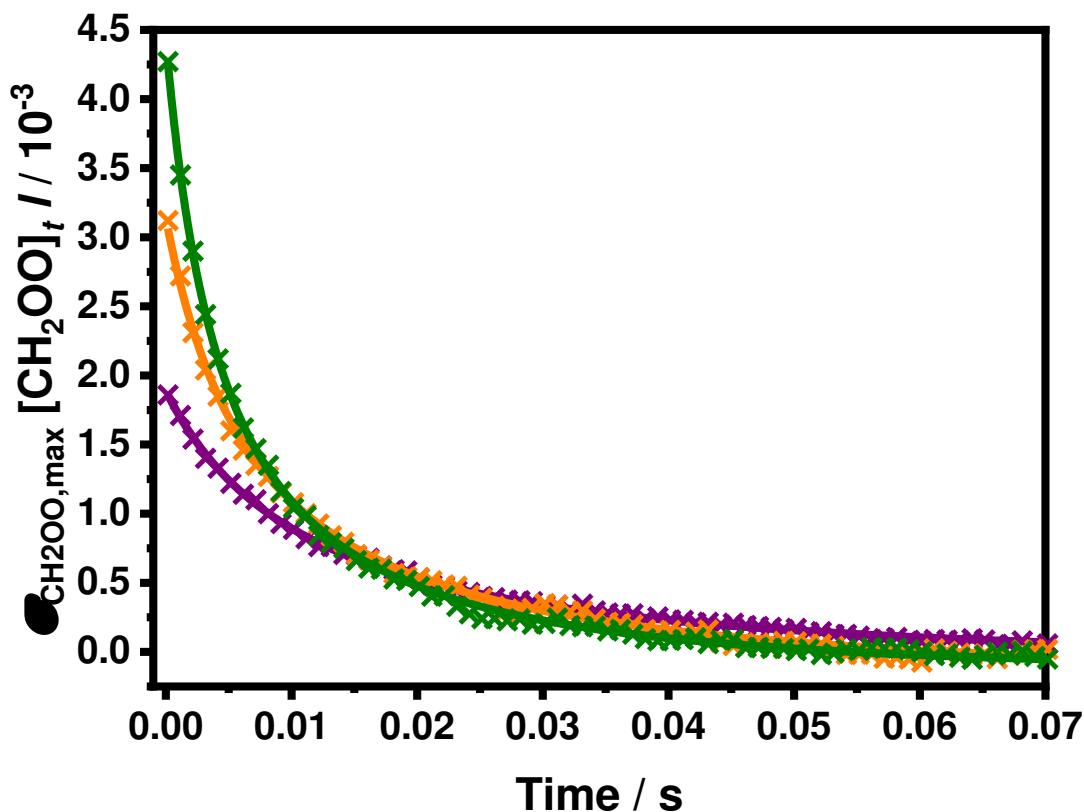


Figure S1: Temporal profile of the product  $\sigma_{\text{CH}_2\text{OO,max}} [\text{CH}_2\text{OO}]_t l = A_{t,\lambda,\text{max}}$  (green, orange and purple points) determined from the observed absorbance at each time point and the respective fit of the mixed order equation (Equation S1, green, orange and purple lines) to the data. For all these data  $p = 70$  Torr. For the data shown in green,  $[\text{O}_2] = 2.19 \times 10^{17} \text{ cm}^{-3}$  and  $[\text{CH}_2\text{I}_2] = 9.72 \times 10^{12} \text{ cm}^{-3}$ , with the fit to the data giving  $A_{0,\lambda,\text{max}} = \sigma_{\text{CH}_2\text{OO,max}} [\text{CH}_2\text{OO}]_{t=0} l = (4.55 \pm 0.03) \times 10^{-3}$ ,  $k_1 = (34.3 \pm 1.3) \text{ s}^{-1}$  and  $k_2 / \sigma_{\text{CH}_2\text{OO,max}} l = (21614 \pm 309) \text{ s}^{-1}$ . For the data shown in orange,  $[\text{O}_2] = 1.49 \times 10^{17} \text{ cm}^{-3}$  and  $[\text{CH}_2\text{I}_2] = 1.91 \times 10^{13} \text{ cm}^{-3}$ , with the fit to the data giving  $A_{0,\lambda,\text{max}} = \sigma_{\text{CH}_2\text{OO,max}} [\text{CH}_2\text{OO}]_{t=0} l = (3.31 \pm 0.03) \times 10^{-3}$ ,  $k_1 = (20.6 \pm 2.6) \text{ s}^{-1}$  and  $k_2 / \sigma_{\text{CH}_2\text{OO,max}} l = (19048 \pm 559) \text{ s}^{-1}$ . For the data shown in purple,  $[\text{O}_2] = 1.50 \times 10^{17} \text{ cm}^{-3}$  and  $[\text{CH}_2\text{I}_2] = 7.25 \times 10^{12} \text{ cm}^{-3}$ , with the fit to the data giving  $A_{0,\lambda,\text{max}} = \sigma_{\text{CH}_2\text{OO,max}} [\text{CH}_2\text{OO}]_{t=0} l = (1.94 \pm 0.02) \times 10^{-3}$ ,  $k_1 = (20.6 \pm 2.6) \text{ s}^{-1}$  and  $k_2 / \sigma_{\text{CH}_2\text{OO,max}} l = (19048 \pm 559) \text{ s}^{-1}$ . From the product of the  $\text{CH}_2\text{I}_2$  depletion and path length, for the data shown in green  $\Delta[\text{CH}_2\text{I}_2] l = 6.06 \times 10^{14} \text{ cm}^{-2}$ , for the data shown in orange  $\Delta[\text{CH}_2\text{I}_2] l = 3.89 \times 10^{14} \text{ cm}^{-2}$ , and for the data shown in purple  $\Delta[\text{CH}_2\text{I}_2] l = 2.28 \times 10^{14} \text{ cm}^{-2}$ , and using the pressure dependent  $\text{CH}_2\text{OO}$  yield,  $Y_{\text{CH}_2\text{OO}, p=70 \text{ Torr}} = 0.65$ , the product of the initial concentration of  $\text{CH}_2\text{OO}$  and path length was calculated to be  $[\text{CH}_2\text{OO}]_0 l = 3.96 \times 10^{14} \text{ cm}^{-2}$  for the data shown in green,  $[\text{CH}_2\text{OO}]_0 l = 2.54 \times 10^{14} \text{ cm}^{-2}$  for the data shown in orange, and  $[\text{CH}_2\text{OO}]_0 l = 1.49 \times 10^{14} \text{ cm}^{-2}$  for the data shown in purple.  $\sigma_{\text{CH}_2\text{OO,max}}$  is then calculated from  $\sigma_{\text{CH}_2\text{OO,max}} [\text{CH}_2\text{OO}]_{t=0} l / [\text{CH}_2\text{OO}]_0 l$ .

## Dependence of $\sigma_{\text{CH}_2\text{OO,max}}$ on pressure

Experiments were carried out over the pressure range 6 – 300 Torr. Figure S2 shows the average  $\sigma_{\text{CH}_2\text{OO,max}}$  value determined at each pressure, indicating that there is no significant dependence of the  $\text{CH}_2\text{OO}$  UV absorption cross-sections on pressure.

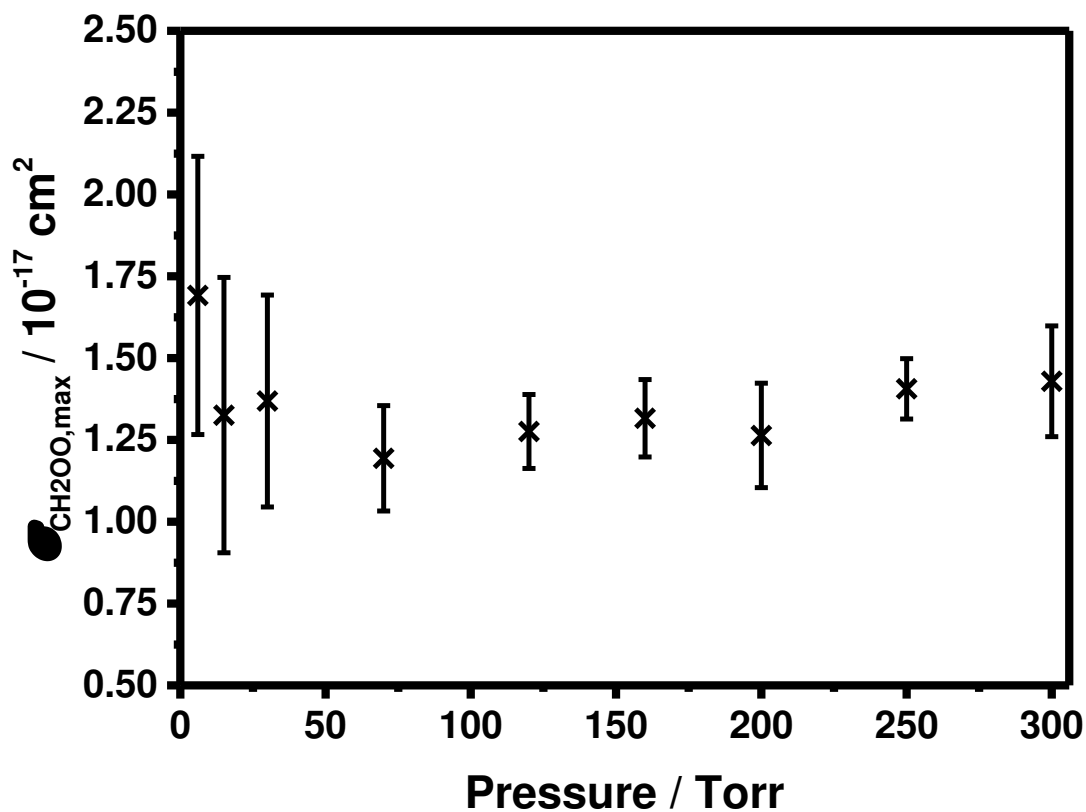


Figure S2: Dependence of  $\sigma_{\text{CH}_2\text{OO,max}}$  on pressure. Results are displayed as the mean value at each pressure, with errors given by the standard deviation of all values at each pressure.

## Absorption cross sections for $\text{CH}_2\text{OO}$ , $\sigma_{\text{CH}_2\text{OO},\lambda}$

Absolute  $\text{CH}_2\text{OO}$  cross-sections from this work in the wavelength range 280 – 450 nm are given in Table S1 below.

Wavelength / nm	Absorption Cross- Section / $10^{-17}$ cm <sup>2</sup>
280.5	0.25
281.1	0.25
281.6	0.25
282.2	0.27
282.8	0.25
283.3	0.28
283.9	0.30
284.5	0.28
285.0	0.29
285.6	0.29
286.2	0.30
286.7	0.31
287.3	0.33
287.9	0.32
288.4	0.36
289.0	0.35
289.6	0.36
290.1	0.38
290.7	0.38
291.3	0.40
291.8	0.38

Wavelength / nm	Absorption Cross- Section / $10^{-17}$ cm <sup>2</sup>
292.4	0.39
293.0	0.40
293.5	0.41
294.1	0.43
294.7	0.47
295.2	0.47
295.8	0.48
296.4	0.48
296.9	0.50
297.5	0.52
298.1	0.53
298.6	0.55
299.2	0.54
299.8	0.56
300.3	0.58
300.9	0.58
301.5	0.60
302.0	0.62
302.6	0.63
303.2	0.64
303.7	0.66

Wavelength / nm	Absorption Cross- Section / $10^{-17}$ cm <sup>2</sup>
304.3	0.67
304.9	0.70
305.4	0.72
306.0	0.73
306.6	0.75
307.1	0.77
307.7	0.78
308.3	0.79
308.8	0.80
309.4	0.82
310.0	0.82
310.5	0.85
311.1	0.88
311.7	0.87
312.3	0.89
312.8	0.90
313.4	0.93
314.0	0.94
314.5	0.95
315.1	0.96
315.7	0.98

Wavelength / nm	Absorption Cross- Section / $10^{-17}$ cm <sup>2</sup>
316.2	0.99
316.8	1.01
317.4	1.02
317.9	1.04
318.5	1.04
319.1	1.06
319.6	1.07
320.2	1.10
320.8	1.10
321.3	1.11
321.9	1.13
322.5	1.14
323.0	1.17
323.6	1.17
324.2	1.18
324.7	1.19
325.3	1.19
325.9	1.22
326.4	1.23
327.0	1.22
327.6	1.25

Wavelength / nm	Absorption Cross- Section / $10^{-17}$ cm <sup>2</sup>
328.1	1.25
328.7	1.26
329.3	1.27
329.8	1.28
330.4	1.28
331.0	1.30
331.5	1.30
332.1	1.31
332.7	1.32
333.2	1.32
333.8	1.34
334.4	1.34
334.9	1.35
335.5	1.34
336.1	1.36
336.6	1.35
337.2	1.35
337.8	1.36
338.3	1.36
338.9	1.36
339.5	1.36

Wavelength / nm	Absorption Cross- Section / $10^{-17}$ cm <sup>2</sup>
340.0	1.37
340.6	1.37
341.2	1.37
341.7	1.38
342.3	1.37
342.9	1.38
343.5	1.37
344.0	1.37
344.6	1.37
345.2	1.36
346.9	1.35
347.4	1.36
348.0	1.36
348.6	1.36
349.1	1.34
349.7	1.34
350.3	1.34
350.8	1.33
351.4	1.32
353.1	1.27
353.7	1.29

Wavelength / nm	Absorption Cross- Section / $10^{-17}$ cm <sup>2</sup>
354.2	1.29
354.8	1.28
355.4	1.28
355.9	1.27
357.6	1.26
358.2	1.23
358.8	1.21
359.3	1.19
359.9	1.19
360.5	1.16
361.0	1.17
361.6	1.16
362.2	1.17
362.7	1.17
363.3	1.18
363.9	1.17
364.4	1.16
365.0	1.14
365.6	1.11
366.1	1.08
366.7	1.03

Wavelength / nm	Absorption Cross- Section / $10^{-17}$ cm <sup>2</sup>
368.4	0.97
369.0	0.97
369.5	0.99
370.1	1.00
370.7	1.02
371.2	1.02
371.8	1.01
372.4	0.99
372.9	0.96
373.5	0.92
374.1	0.88
374.7	0.85
375.2	0.81
375.8	0.80
376.4	0.78
376.9	0.78
377.5	0.78
379.2	0.84
379.8	0.84
380.3	0.83
380.9	0.81

Wavelength / nm	Absorption Cross- Section / $10^{-17}$ cm <sup>2</sup>
381.5	0.77
382.0	0.74
382.6	0.69
383.2	0.64
383.7	0.61
384.3	0.57
384.9	0.57
385.4	0.57
386.0	0.58
386.6	0.59
387.1	0.63
387.7	0.65
388.3	0.66
390.0	0.61
390.5	0.56
391.1	0.53
391.7	0.49
392.2	0.45
392.8	0.42
394.5	0.40
395.1	0.39

Wavelength / nm	Absorption Cross- Section / $10^{-17}$ cm <sup>2</sup>
395.6	0.41
396.2	0.43
396.8	0.44
397.3	0.47
397.9	0.46
398.5	0.46
399.0	0.44
400.7	0.37
401.3	0.33
401.9	0.31
402.4	0.28
403.0	0.26
403.6	0.25
405.3	0.26
405.9	0.27
406.4	0.28
407.0	0.30
407.6	0.31
408.1	0.30
408.7	0.31
409.3	0.31

Wavelength / nm	Absorption Cross- Section / $10^{-17}$ cm <sup>2</sup>
409.8	0.27
410.4	0.25
411.0	0.25
411.5	0.21
412.1	0.19
412.7	0.18
413.2	0.18
413.8	0.17
414.4	0.16
416.1	0.17
416.6	0.16
417.2	0.17
417.8	0.18
418.3	0.18
418.9	0.17
419.5	0.17
420.0	0.16
420.6	0.16
421.2	0.16
421.7	0.15
422.3	0.15

Wavelength / nm	Absorption Cross- Section / $10^{-17}$ cm <sup>2</sup>
422.9	0.14
423.4	0.14
424.0	0.12
424.6	0.11
425.1	0.12
426.8	0.07
427.4	0.06
428.0	0.08
428.5	0.09
429.1	0.09
429.7	0.10
430.2	0.11
430.8	0.12
431.4	0.12
431.9	0.12
432.5	0.11
433.1	0.10
433.6	0.10
434.2	0.09
434.8	0.08
435.4	0.06

Wavelength / nm	Absorption Cross- Section / $10^{-17}$ cm <sup>2</sup>	Wavelength / nm	Absorption Cross- Section / $10^{-17}$ cm <sup>2</sup>
435.9	0.05	443.9	0.08
437.6	0.06	444.4	0.06
438.2	0.07	445.0	0.05
438.8	0.08	445.6	0.05
439.3	0.08	446.1	0.05
439.9	0.06	446.7	0.07
440.5	0.07	447.3	0.06
441.0	0.06	447.8	0.05
441.6	0.06	448.4	0.05
442.2	0.06	449.0	0.04
442.7	0.07	449.5	0.05
443.3	0.07		

Table S1: Summary of CH<sub>2</sub>OO absorption cross-sections.

## Dependence of IO concentration on the initial CH<sub>2</sub>I concentration

Concentration-time profiles for IO radicals indicate an initial rapid production of IO, occurring within 1 ms of photolysis, which is followed by further slower production of IO (see main text). Figure S3 shows the dependence of the observed initial IO concentrations, produced within 1 ms of photolysis, and the maximum IO concentrations observed, on the initial concentrations of CH<sub>2</sub>I radicals. The initial concentration of CH<sub>2</sub>I in the system, [CH<sub>2</sub>I]<sub>0</sub>, was determined from the observed depletion in CH<sub>2</sub>I<sub>2</sub> absorbance. Concentrations of the IO radicals produced in the initial rapid process, [IO]<sub>t=1 ms</sub>, were observed to be directly proportional to [CH<sub>2</sub>I]<sub>0</sub> (Figure S3a), with a yield of rapid IO formation of (14.8 ± 0.5) % of the initial CH<sub>2</sub>I concentration. Similarly, the maximum IO concentrations, [IO]<sub>max</sub>, were also observed to be directly proportional to [CH<sub>2</sub>I]<sub>0</sub> (Figure S3b), with an IO yield of (17.2 ± 0.5) % of the initial CH<sub>2</sub>I concentration.

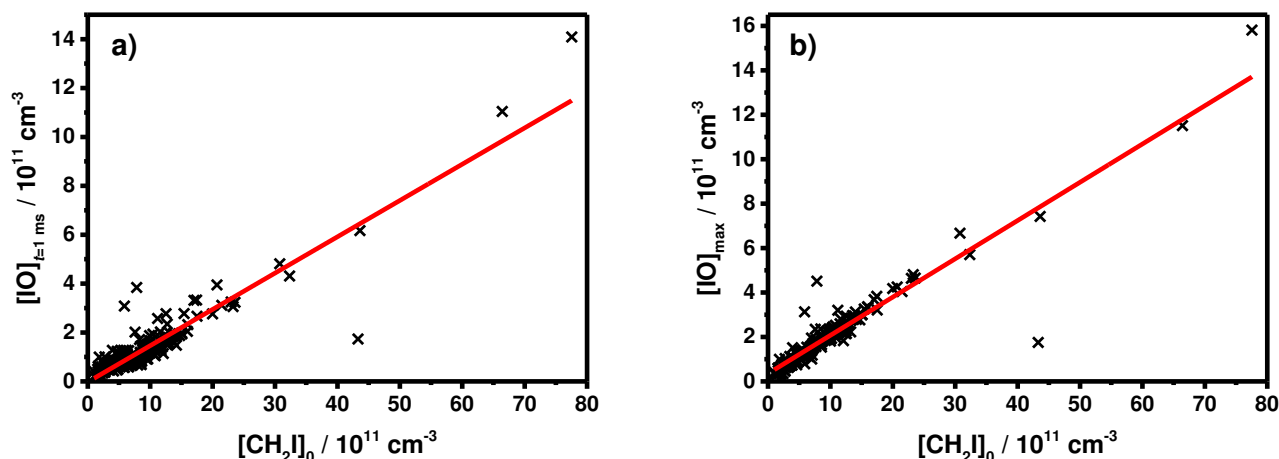


Figure S3: Relationships between a) the concentrations of IO produced within 1 ms of photolysis and the initial concentrations of CH<sub>2</sub>I, and b) the maximum concentrations of IO and the initial concentrations of CH<sub>2</sub>I. Linear fits to the data (red lines) give a) gradient = (14.8 ± 0.5) and intercept = (-2.3 ± 6.1) × 10<sup>9</sup> cm<sup>-3</sup> and b) gradient = (17.2 ± 0.5) and intercept = (3.5 ± 0.6) × 10<sup>10</sup> cm<sup>-3</sup>.

## Comparison of observed and simulated IO profiles

Simulated IO profiles, constrained to the initial observed IO concentrations, in which the reaction of  $\text{CH}_2\text{OO} + \text{I}$  exclusively produced  $\text{CH}_2\text{IO}_2$  were compared to observed IO time profiles. The results suggested that both the production and decay of IO in the system are underestimated in the model as listed in Table 2 in the main text. Simulations in which rate coefficients for the  $\text{CH}_2\text{IO}_2$  self-reaction ( $k_6$ ) and the  $\text{CH}_2\text{IO}_2 + \text{I}$  reaction ( $k_7$ ) were systematically increased and decreased show that the discrepancy between observed and simulated IO may be due to uncertainties in  $\text{CH}_2\text{IO}_2$  peroxy radical chemistry. On average, an increase of a factor of 3 in the rate coefficient for the  $\text{CH}_2\text{IO}_2$  self-reaction and of a factor of approximately 2 in the rate coefficient for the  $\text{CH}_2\text{IO}_2 + \text{I}$  reaction was required in order to simulate an IO profile in agreement with the observed IO. A comparison between observed and simulated IO profiles for data at 70 Torr is given in Figure 8 in the main text, and Figure S4 shows this comparison for data at 300 Torr. These results suggest that kinetics of  $\text{CH}_2\text{IO}_2$  chemistry in the model need to be altered in order to account for the observed IO in the system.

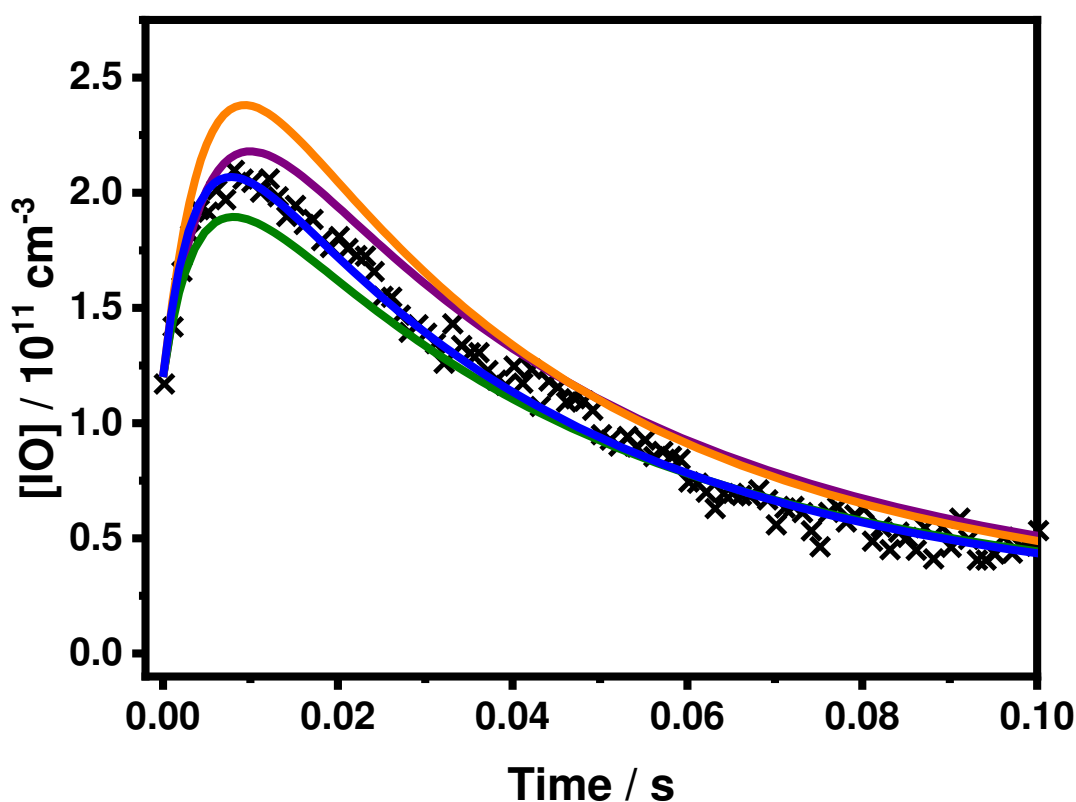


Figure S4: Experimentally observed IO concentrations (black points) and simulated IO profiles using the mechanism given in Table 2 in the main text, except where specified otherwise, and constrained to the observed IO concentration at  $t = 1$  ms. The reaction between  $\text{CH}_2\text{OO}$  and I (R4 in the main text) was set to produce  $\text{CH}_2\text{IO}_2$  with 100 % yield (purple). Adjustments made to the rate coefficients of the  $\text{CH}_2\text{IO}_2$  self-reaction (R6 in the main text) and the  $\text{CH}_2\text{IO}_2 + \text{I}$  reaction (R7 in the main text) to simulate IO profiles which better represented the IO observed in the system than using rate coefficients as given in Table 2 in the main text were  $2.75 \times k_6$  (green),  $1.25 \times k_7$  (orange) and a combination of both  $2.75 \times k_6$  and  $1.25 \times k_7$  (blue). For these data,  $p = 300$  Torr,  $[\text{O}_2] = 1.76 \times 10^{17} \text{ cm}^{-3}$ ,  $[\text{CH}_2\text{I}_2] = 1.30 \times 10^{13} \text{ cm}^{-3}$ , and  $[\text{CH}_2\text{OO}]_0 = 3.50 \times 10^{11} \text{ cm}^{-3}$ .

## Sensitivity of the system to CH<sub>2</sub>OO + IO

Potential impacts of any reaction between CH<sub>2</sub>OO and IO on the analysis used to determine the kinetics for the CH<sub>2</sub>OO self-reaction ( $k_3$ ) and for the reaction between CH<sub>2</sub>OO and I ( $k_4$ ) were investigated through a series of model fits in which a reaction between CH<sub>2</sub>OO and IO was included in the mechanism. Fits were performed with the rate coefficient for CH<sub>2</sub>OO + IO fixed to a series of values between  $1 \times 10^{-11}$  and  $1 \times 10^{-10}$  cm<sup>3</sup> s<sup>-1</sup>, with the mechanism otherwise as shown in Table 2 in the main text and the initial IO concentration constrained to the observed value. Figure S5 shows the impacts on the fit results for  $k_3$  and  $k_4$ . For the largest rate coefficient adopted in the model for CH<sub>2</sub>OO + IO, the fit results for  $k_3$  and  $k_4$  are within 15 % of the values obtained from model fits in which CH<sub>2</sub>OO + IO is not considered, with the loss of IO dominated by the IO self-reaction. Results for  $k_3$  and  $k_4$  reported in this work are thus given from fits performed in which CH<sub>2</sub>OO + IO is not considered.

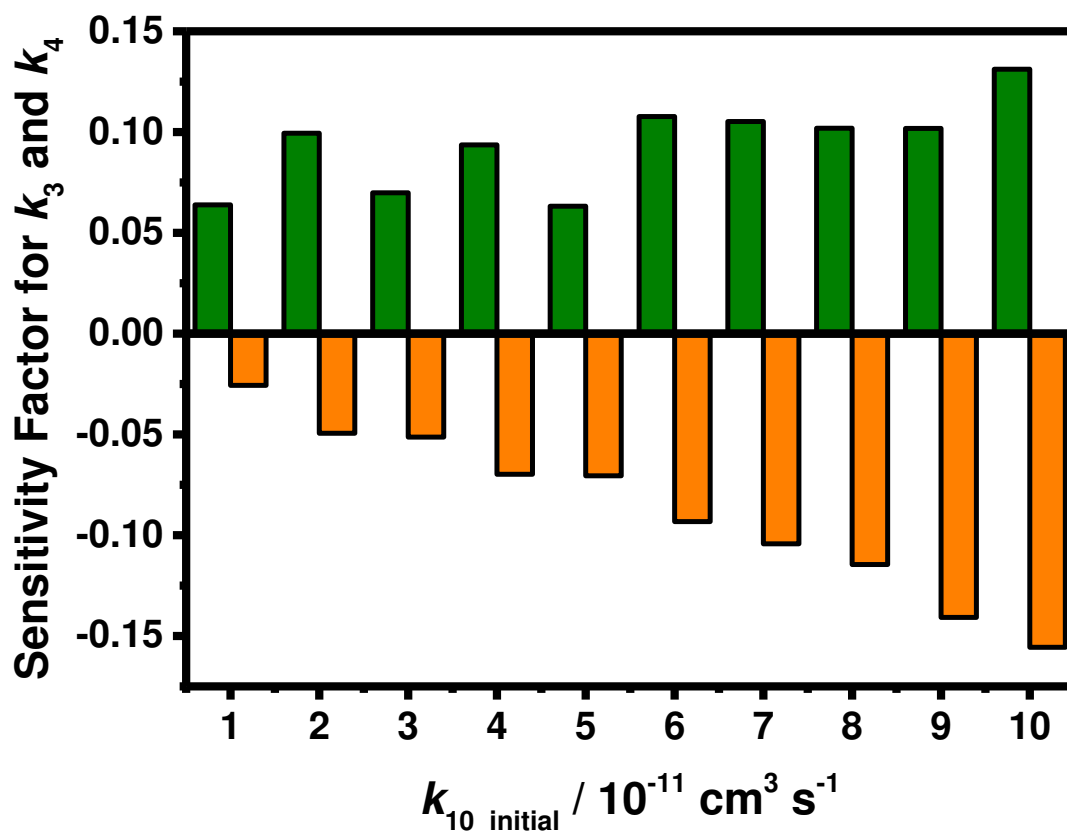


Figure S5: Sensitivity of  $k_3$  (green) and  $k_4$  (orange) to the rate coefficient for CH<sub>2</sub>OO + IO adopted in the model used to fit to experimental observations. Results are shown for model fits performed at  $p = 300$  Torr, at which pressure the effects, if any, of a potential CH<sub>2</sub>OO + IO reaction are expected to be most prevalent due to the high yield of IO in the system (see main text and Figure 9). The sensitivity factors are defined as the fractional difference in the fit result for the rate coefficient compared to the result obtained for fits in which CH<sub>2</sub>OO + IO is not considered.